

NUMERICAL SIMULATION OF DOI MODEL OF POLYMERIC FLUIDS

RUO LI *, CHONG LUO* , AND PINGWEN ZHANG*

Abstract. We study the Doi model for shear flow. The finite element method on sphere is developed, the basis function is carefully chosen to guarantee the conservation of distribution function. The numerical results presented confirm the main conclusion. The viscosity jump is observed during the flow induced phase transition.

Key words. Doi model, shear flow, kayaking, log-rolling, viscosity, FEM, sphere, Voronoi.

AMS subject classifications.

1. Introduction. Viscoelastic liquids have been known for many years to display striking difference to Newtonian fluids in a variety of flow situations [1, 2]. The viscoelastic properties of polymers are quite important in polymer industry. They are related to the molecular dynamics and depend on molecular weight, concentration and molecular structure.

Polymer molecular models are generally nonlinear and have large numbers of internal degrees of freedom, which make simulating these molecular models both numerically challenging and fundamentally important. Most micromechanical models used in the kinetic theory of polymeric liquids consist of collections of beads joined together by elastic springs or rigid rods. For dilute polymer solutions, elastic dumbbell models have been exclusively used for complex flow simulations. For the rod-like polymer such as liquid crystalline polymer, a rigid dumbbell model (the Doi model) is the most commonly used model.

The rigid rod model is capable of predicting several rheological features of rodlike polymers in the nematic phase [5, 7]. A homogeneous population of equal rods is described with an orientational distribution function. The evolution of the distribution function is modeled with Fokker-Planck (Smoluchowski) equation. The rheological response is determined once the distribution is known.

Spherical harmonics were used as basis functions to simulate the Fokker-Planck equation for rodlike polymers [12]. They are the eigenfunctions of the operator in the Fokker-Planck equation at $De = 0$, where De is the Deborah number that describes the relative time scales of molecular relaxation and of the flow field. However, if De is large or if the diffusion coefficient depends on the configuration operators in the Fokker-Planck equation, the spherical harmonics are no longer efficient. Observing that for large De the distribution function is a highly localized function, Nayak [14] proposed using wavelets as alternative basis functions to spherical harmonics.

Marrucci and Maffettone [8] performed the first simulation of the Doi model without a closure approximation for simple shear flow. They assumed that all of the molecules lie within the shear plane and thereby reduced the model to only one dimension.

$$\frac{\partial \psi}{\partial t} = \frac{1}{De} \frac{\partial}{\partial \theta} \left(\frac{\partial \psi}{\partial \theta} + \psi \frac{\partial \tilde{V}}{\partial \theta} \right) + \Gamma \frac{\partial}{\partial \theta} (\psi \sin^2 \theta),$$

where $\psi(\theta, t)$ is the distribution function, θ is parameter angle in the circle and $\Gamma = u_y$

*LMAM and School of Mathematical Sciences, Peking University, Beijing 100871, P.R.China.

is the constant shear rate,

$$\bar{V}(\theta, t) = \frac{3}{2}U \int_0^{2\pi} \sin^2(\theta - \theta')\psi(\theta', t)d\theta'.$$

Even with this simplified model, they observed tumbling dynamics in the simulation. When U increases, the equilibrium distribution becomes peaked and tumbling appears. However, when increasing the shear rate Γ , the tumbling eventually disappears. Larson [9] and Larson and Ottinger [12] used spherical harmonics to simulate the evolution of Doi model using Onsager potential in two dimensions, also for simple shear flow. They have shown that the rigid-rod model is indeed capable of predicting most of the rheological response of polymers in the nematic phase, including the existence of ranges of shear rates with negative values of the first normal stress difference, dynamics within the flow plane as well as additional out-of-plane dynamics such as log rolling and kayaking. Their numerical results also confirmed the main conclusion of Marrucci and Maffettone [8], namely, that shearing at a high enough rate can significantly distort the distribution function function, making it less anisotropic. The detailed description of the bifurcation structures of the model is delivered by Faraoni, Grosso, Crescitelli and Maffettone [6].

Doi Model is extended to properly take into account the local interactions between rods in an inhomogeneous system in [20], which is used to study the microstructure formation, disclination dynamics and polydomain texture for liquid crystal polymers undergoing shear flow.

2. The Doi Model . The Doi model is an extension of earlier work by Onsager, Maier and Saupe on equilibrium behavior of rod-like molecules to the study of dynamics [7]. For homogeneous systems the order parameter in these models in the one-particle distribution function function of the rods, denoted by $\psi(\mathbf{m}, t)$. Interaction between the rods is modeled via the excluded volume effect, giving rise to a mean-field Onsager potential

$$V(\mathbf{m}) = \frac{3}{2}Uk_B T \int_{S^2} |\mathbf{m} \times \mathbf{m}'| \psi(\mathbf{m}') d\mathbf{m}'$$

or the Maier–Saupe potential

$$V(\mathbf{m}) = \frac{3}{2}Uk_B T \int_{S^2} |\mathbf{m} \times \mathbf{m}'|^2 \psi(\mathbf{m}') d\mathbf{m}',$$

where S^2 denotes the unit sphere, $k_B T$ is the Boltzmann factor. The Fokker-Planck equation is then

$$\frac{\partial \psi}{\partial t} + \nabla_{\mathbf{x}} \cdot (\mathbf{u}\psi) = D_r \mathcal{R} \cdot (\mathcal{R}\psi + \frac{\psi}{k_B T} \mathcal{R}V) - \mathcal{R} \cdot (\mathbf{m} \times \kappa \mathbf{m}\psi),$$

where $D_r = \frac{1}{\xi_r}$, where \mathbf{u} is the velocity field, ξ_r is the rotational friction coefficient, $\kappa = (\nabla \mathbf{u})^T$, and

$$\mathcal{R} = \mathbf{m} \times \frac{\partial}{\partial \mathbf{m}}$$

is the rotational derivative operator.

The velocity field satisfies a Navier-Stokes-like equation:

$$\begin{cases} \frac{\partial \mathbf{u}}{\partial t} + (\mathbf{u} \cdot \nabla) \mathbf{u} = \frac{1}{\rho} (-\nabla p + \nabla \cdot \boldsymbol{\tau}) \\ \nabla \cdot \mathbf{u} = 0, \end{cases}$$

where $\boldsymbol{\tau}$ is the stress tensor with contributions from the solvent $\boldsymbol{\tau}^s$, and the rods $\boldsymbol{\tau}^p$:

$$\boldsymbol{\tau} = \boldsymbol{\tau}^s + \boldsymbol{\tau}^p,$$

$\boldsymbol{\tau}^s$ can be modeled by the standard linear constitutive relation:

$$\boldsymbol{\tau}^s = \eta_s (\boldsymbol{\kappa} + \boldsymbol{\kappa}^T),$$

η_s is the solvent viscosity, and $\boldsymbol{\tau}^p$ is the elastic tensor, can be computed from

$$\begin{aligned} \tau_{\alpha\beta}^p &= 3\nu k_B T S_{\alpha\beta} - \nu \langle (\mathbf{m} \times \mathcal{R}V)_\alpha m_\beta \rangle \\ &\quad + \frac{\nu}{2} \xi_r \kappa_{\mu\nu} \langle m_\alpha m_\beta m_\mu m_\nu \rangle \\ S_{\alpha\beta} &= \langle m_\alpha m_\beta - \frac{1}{3} \delta_{\alpha\beta} \rangle, \end{aligned}$$

here we have used $\langle \ \rangle$ to denote averaging with respect to the distribution function ψ .

Let L_0 be the typical size of the flow region, V_0 be the typical velocity scale, $T_0 = \frac{L_0}{V_0}$ be a typical convective time scale. We can then non-dimensionalize these equations, and obtain

$$\frac{\partial \psi}{\partial t} + \nabla_{\mathbf{x}} \cdot (\mathbf{u}\psi) = \frac{1}{De} \mathcal{R} \cdot (\mathcal{R}\psi + \psi \mathcal{R}\tilde{V}) - \mathcal{R}(\mathbf{m} \times \boldsymbol{\kappa} \mathbf{m} \psi), \quad (2.1)$$

here $\tilde{V} = \frac{V}{k_B T}$, De is an important parameter called the Deborah number

$$De = \frac{\frac{\xi_r}{k_B T}}{\frac{L_0}{V_0}} = \frac{\xi_r V_0}{k_B T L_0},$$

it is the ratio of the orientational diffusion time scale of the rods (which is the relevant relaxation time scale) and the convective time scale of the fluid.

Let

$$\eta_p = \nu \xi_r, \quad \eta = \eta_s + \eta_p, \quad \gamma = \frac{\eta_s}{\eta}.$$

We can then non-dimensionalize the Navier-Stokes-like equation to get

$$\frac{\partial \mathbf{u}}{\partial t} + (\mathbf{u} \cdot \nabla) \mathbf{u} + \nabla p = \frac{\gamma}{Re} \Delta \mathbf{u} + \frac{1-\gamma}{De Re} \nabla \cdot \boldsymbol{\tau}^p, \quad (2.2)$$

where

$$\begin{aligned} \tau_{\alpha\beta}^p &= 3S_{\alpha\beta} - \langle (\mathbf{m} \times \mathcal{R}\tilde{V})_\alpha m_\beta \rangle \\ &\quad + \frac{De}{2} \kappa_{\mu\nu} \langle m_\alpha m_\beta m_\mu m_\nu \rangle \\ S_{\alpha\beta} &= \langle m_\alpha m_\beta - \frac{1}{3} \delta_{\alpha\beta} \rangle. \end{aligned} \quad (2.3)$$

3. The Finite Element Method on Sphere. The orientation of a rod is determined by a unit pseudo-vector \mathbf{m} , or equivalently by two angles ϑ and ϕ . The distribution function $\psi(\mathbf{m}, t)$ gives the probability density that a rod is oriented along \mathbf{m} at time t . The diffusion equation for the distribution function is Fokker-Planck equation (2.1)

$$\frac{\partial \psi}{\partial t} = \frac{1}{De} \mathcal{R} \cdot (\mathcal{R}\psi + \psi \mathcal{R}\tilde{V}) - \mathcal{R}(\mathbf{m} \times \kappa \mathbf{m} \psi), \quad (3.1)$$

and

$$\tilde{V} = \frac{3}{2}U(1 - \mathbf{m}\mathbf{m} : \langle \mathbf{m}\mathbf{m} \rangle)$$

where the convection term disappears because we only consider the shear flow, U is the nondimensional potential intensity. Here we consider the shear flow with velocity oriented along the direction 1, and the gradient of the velocity oriented along the direction 3,

$$\kappa = \begin{pmatrix} 0 & 0 & \dot{\gamma} \\ 0 & 0 & 0 \\ 0 & 0 & 0 \end{pmatrix}. \quad (3.2)$$

The equation (3.1) can be made nondimensional through the rational diffusivity when we only consider the Fokker-Planck equation, so that the time becomes t/De , and the shear rate becomes $G = \dot{\gamma}De$. Thus, two nondimensional parameters appear in the equation: the intensity of the nematic field U and the shear rate G .

A number of problems are encountered when one tries to numerically solve differential equations in spherical geometry. These difficulties, collectively known as pole problems, can arise from the use of a particular coordinate system and from trying to discretize the surface of the sphere. An early alternative to spherical coordinates was to project the equations from the sphere to a plane. The surface of a sphere and that of a plane are not topologically equivalent. Williamson [19] and Sadourny et al. [17] simultaneously introduced a new approach to more isotropically and homogeneously discretize the sphere. Their grids are constructed from spherical triangles that are nearly equal in area and that are nearly equilateral. The grid is called a spherical geodesic grid. We will develop finite element method based on spherical geodesic grid to solve the Fokker-Planck equation.

3.1. Voronoi spherical geodesic grid. We use Voronoi method [3] to generate the spherical geodesic grid. Voronoi method enjoys the advantage of generating cells that are nearly equal in area and that are nearly equilateral.

Figure 3.1 shows a grid generated using Voronoi method, on which there are totally 800 nodes. This grid is the one we have used in the following numerical results.

3.2. Basis functions. We will project the linear basis functions of the triangles on the polyhedron onto the spherical geodesic triangles. The vertices (anti-clockwise) of a spherical geodesic triangle $\hat{\Delta}$ are denoted by A, B and C , the plane triangle Δ has the same vertices, P is a point on $\hat{\Delta}$, the intersection point OP with triangle Δ is denoted by W ,

$$OA = \mathbf{a}_1, \quad OB = \mathbf{a}_2, \quad OC = \mathbf{a}_3, \quad OP = \mathbf{m}, \quad OW = \mathbf{w}.$$

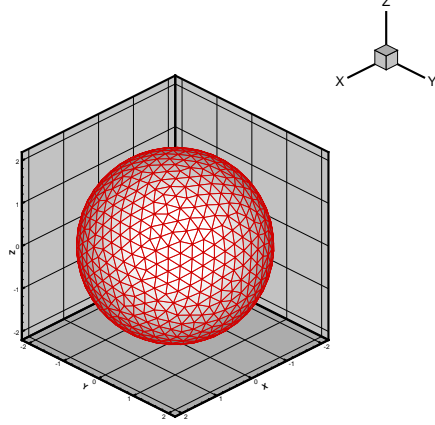


FIG. 3.1. The Voronoi spherical geodesic grid we have used. On this grid, there are totally 800 nodes, 1596 elements and 2394 sides.

We define the basis functions on spherical geodesic triangle $\hat{\Delta}$

$$\begin{aligned}\lambda_1(\mathbf{m}) &= \frac{1}{D}(\mathbf{w} \cdot \mathbf{a}_2 \times \mathbf{a}_3), \\ \lambda_2(\mathbf{m}) &= \frac{1}{D}(\mathbf{w} \cdot \mathbf{a}_3 \times \mathbf{a}_1), \\ \lambda_3(\mathbf{m}) &= \frac{1}{D}(\mathbf{w} \cdot \mathbf{a}_1 \times \mathbf{a}_2),\end{aligned}\tag{3.3}$$

where

$$D = (\mathbf{a}_1 \cdot \mathbf{a}_2 \times \mathbf{a}_3), \quad \mathbf{w}(\mathbf{m}) = D \frac{\mathbf{m}}{\mathbf{m} \cdot \mathbf{d}}$$

and

$$\mathbf{d} = (\mathbf{a}_1 \times \mathbf{a}_2 + \mathbf{a}_2 \times \mathbf{a}_3 + \mathbf{a}_3 \times \mathbf{a}_1).$$

Then we have

$$\lambda_1(\mathbf{m}) = \frac{\mathbf{m} \cdot \mathbf{a}_2 \times \mathbf{a}_3}{\mathbf{m} \cdot \mathbf{d}},$$

and

$$\begin{aligned}\mathcal{R}\lambda_1(\mathbf{m}) &= \frac{1}{(\mathbf{m} \cdot \mathbf{d})^2} \{(\mathbf{m} \times \mathbf{a}_2 \times \mathbf{a}_3)(\mathbf{m} \cdot \mathbf{d}) - (\mathbf{m} \cdot \mathbf{a}_2 \times \mathbf{a}_3)(\mathbf{m} \times \mathbf{d})\} \\ &= \frac{1}{D}(\mathbf{w} \times \mathbf{a}_2 \times \mathbf{a}_3) - \frac{1}{D}\lambda_1(\mathbf{m})(\mathbf{w} \times \mathbf{d}).\end{aligned}$$

$\mathcal{R}\lambda_2(\mathbf{m})$ and $\mathcal{R}\lambda_3(\mathbf{m})$ could be similarly obtained. It is easy to verify that

$$\lambda_1(\mathbf{m}) + \lambda_2(\mathbf{m}) + \lambda_3(\mathbf{m}) \equiv 1,\tag{3.4}$$

$$\mathcal{R}\lambda_1(\mathbf{m}) + \mathcal{R}\lambda_2(\mathbf{m}) + \mathcal{R}\lambda_3(\mathbf{m}) \equiv 0.\tag{3.5}$$

With the given shape functions on the element, we then obtain the finite element space H_h on the triangulation on the sphere. Let's denote $H^1(\Omega)$ as the Hilbert space on the sphere with the norm

$$\|f\|_{H^1(\Omega)}^2 := \|f\|_{L^2(\Omega)}^2 + \|\mathcal{R}f\|_{L^2(\Omega)}^2, \quad (3.6)$$

H_h then is a subspace of $H^1(\Omega)$. The function in H_h is in C^0 space.

3.3. Weak formulation. The weak formation of the Fokker-Planck equation while $\dot{\gamma} = 0$: find $\psi \in H^1(\Omega)$, $\psi \geq 0$, $\|\psi\|_{L^1(\Omega)} = 1$, such that

$$\int_{\Omega} \frac{\partial \psi}{\partial t} v dx + \frac{1}{De} \int_{\Omega} \mathcal{R}\psi \cdot \mathcal{R}v dx = -\frac{1}{De} \int_{\Omega} \psi \mathcal{R}\tilde{V}(\psi) \cdot \mathcal{R}v dx, \forall v \in H^1(\Omega). \quad (3.7)$$

In the finite element space, the semi-implicit approximation to the weak formation is: find $\psi_h^n \in H_h$, $\psi_h^n \geq 0$, $\|\psi_h^n\|_{L_h^1(\Omega)} = 1$, such that

$$\int_{\Omega} \frac{\psi_h^{n+1} - \psi_h^n}{\Delta t} v_h dx + \frac{1}{De} \int_{\Omega} \mathcal{R}\psi_h^{n+1} \cdot \mathcal{R}v_h dx = -\frac{1}{De} \int_{\Omega} \psi_h^n \mathcal{R}\tilde{V}(\psi_h^n) \cdot \mathcal{R}v_h dx, \forall v_h \in H_h. \quad (3.8)$$

The difference from solving a common heat equation is that the stiff matrix and mass matrix for the system can only be obtained by numerical quadrature formula, but not by exact formula. We construct the transformation from the unit triangle to the spherical triangle in two steps: first, we map the unit triangle to the plane triangle with its vertex same as the spherical triangle, this is a linear transformation, denoted by L ; and second, we map the plane triangle to the spherical triangle with: $N : \mathbf{a} \mapsto \frac{\mathbf{a}}{|\mathbf{a}|}$. The jacobian determinant of the transformation NL can be easily obtained. Then a quadrature on the spherical triangle can be calculated as

$$\begin{aligned} \int_{\Delta} f(\mathbf{m}) d\mathbf{m} &= \int_{\Delta_I} f(N(L(\xi))) \det(NL) d\xi \\ &\cong \sum_{q_i} w_i f(N(L(q_i))) \det(NL)|_{q_i} |\Delta_I|, \end{aligned}$$

in which Δ_I is the unit triangle, q_i are numerical quadrature points, and w_i are corresponding to quadrature weights. In virtue of the identity (3.4) and (3.5), we can get the conservation

$$\|\psi_h^{n+1}\|_{L_h^1(\Omega)} = \|\psi_h^n\|_{L_h^1(\Omega)}.$$

4. Numerical results . The results presented in this work have been obtained by using finite element method for Fokker-Planck equation on sphere. The Voronoi spherical geodesic grid [3] we have used consists of 800 nodes on the unit sphere.

We have taken the advantage of parallel computing to simulate many cases simultaneously. All the computations are done on LSSCII of Chinese Academy of Science, each node of which consists of two Intel 2GHz Xeon processors and 1GB memory. Even with this super computer, it typically takes 48 hours to simulate 100 cases simultaneously for 200,000 time steps on 25 nodes using 50 processors.

For the sake of clarity, we first illustrate the equilibrium situation, that is stationary solutions at rest. At equilibrium, the scalar order parameter, can be calculated by

$$S = \frac{3}{2}\lambda$$

where λ is the eigenvalue with largest absolute value of the traceless second-rank order \mathbf{S} tensor given by

$$\mathbf{S} = \langle \mathbf{m}\mathbf{m} \rangle - \frac{1}{3}\mathbf{I},$$

with \mathbf{I} as the second-rank unit tensor. The director is the eigenvector corresponding to λ , and is used to denote the average molecular direction. The scalar order parameter is zero when the system is isotropic. It is positive in the case of prolate distributions, and negative for oblate ones. Figure 4.1 shows the scalar order parameter S versus

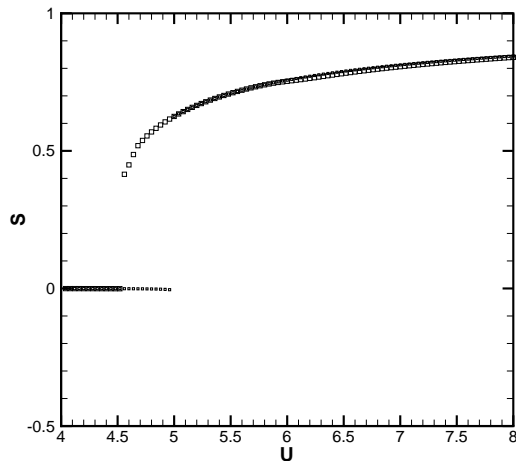


FIG. 4.1. *The equilibrium value of the scalar order parameter S .*

the potential intensity U for two different initial data, one is isotropic, the other with the initial director in the $y-z$ plane and the angle is $\frac{\pi}{8}$ with z -axis. Here, our initial distribution function is

$$\psi(\mathbf{m}, 0) = \frac{1}{4\pi} + \frac{1}{16} \sqrt{\frac{5}{\pi}} (3(\mathbf{m}_0^T \mathbf{m})^2 - 1), \quad (4.1)$$

where \mathbf{m}_0 is unit vector. It is easy to verify that the director of (4.1) is \mathbf{m}_0 . In figure 4.1, two solution branches cross at a transcritical bifurcation point for $U = U_2 = 5$, a limit point is encountered in the nematic branch for $U = U_1 = 4.49$. Thus for $U < U_1$ only a stable isotropic phase is predicted, for $U_1 < U < U_2$, two nematic solutions (one stable and the other unstable) and one stable isotropic solution are predicted. Both those nematic solutions are prolate. For $U > U_2$ three solutions coexist as well, a stable prolate solution ($S > 0$), an unstable isotropic solution, and a stable oblate nematic solution ($S < 0$) (It is worth noting that this prediction of stable oblate solution is different from that of [6], please check [4] for detail).

The solutions when the shear flow is present are described by plotting two different descriptors of the state of the system versus the shear rate G . One descriptor is the real part of b_{22} , the other is the imaginary part of b_{22} , where b_{22} is the coefficient of

the spherical harmonic $Y_{2,2}$ of distribution function ψ . It is easy to verify that

$$\langle \mathbf{mm} \rangle_{11} - \langle \mathbf{mm} \rangle_{22} = 4\sqrt{\frac{2\pi}{15}} \text{Re}[b_{2,2}] \quad (4.2)$$

$$\langle \mathbf{mm} \rangle_{12} = -2\sqrt{\frac{2\pi}{15}} \text{Im}[b_{2,2}] \quad (4.3)$$

The former quantity is zero at isotropy. The imaginary part clearly describes out-of-plane solutions, since it is nonzero when solutions are not symmetric with respect to the shear plane. Figure 4.2 shows the solution diagram for $U = 4.45$ versus the shear rate G , it is apparent that the flow induces a phase transition.

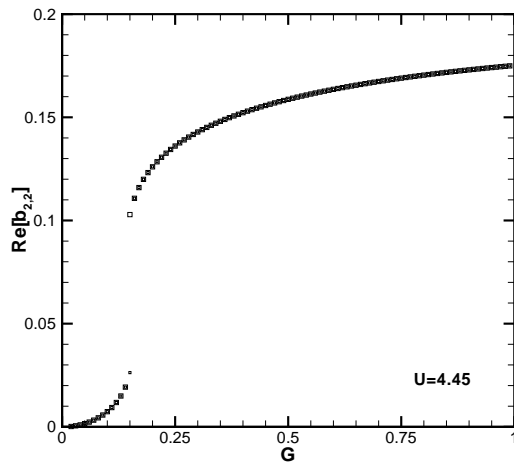


FIG. 4.2. $\text{Re}[b_{22}]$ vs shear rate for $U=4.45$

Figure 4.3 to 4.6 show the solution diagram for $U = 5.33$. It is apparent that the situation is very complex. We illustrate the various possibilities for the evolution of structure parameters, including dynamics within the shear plane as well as additional out-of-plane dynamics such as log rolling and kayaking. Those rich and interesting dynamics and bifurcation behavior are also revealed by Faraoni et al. [6] and Nayak [14].

Figure 4.7 and 4.8 show the distribution function of flow-aligning and log-rolling. In these figures, we can clearly see that the director indeed represents the average molecule direction. Figure 4.9 to figure 4.11 show the evolution of directors for these solutions: tumbling, wagging, out of plane oscillating, log-rolling and kayaking. These figures give us good intuition about why these solutions are so called.

It has been observed that [9], as shear rate increases, several transitions of solution types occur. The first transition is from tumbling to wagging, the second is from wagging to flow-aligning. Each transition is associated with a predicted change in sign of the time average value of $N_1 = \tau_{11} - \tau_{33}$. As the shear rate increases, the time average value of N_1 is predicted to change from positive to negative, and then back to positive. For fluids that are isotropic at equilibrium, $N_2 = \tau_{33} - \tau_{22}$ has always been found to be negative or zero [9] and considerably smaller in magnitude than N_1 .

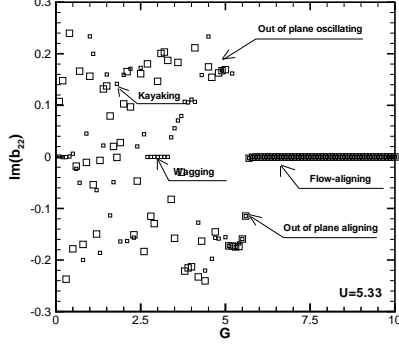


FIG. 4.3. Snapshot of $Im[b_{22}]$ at time $t = 2000$ for two different initial distribution functions for $U = 5.33$.

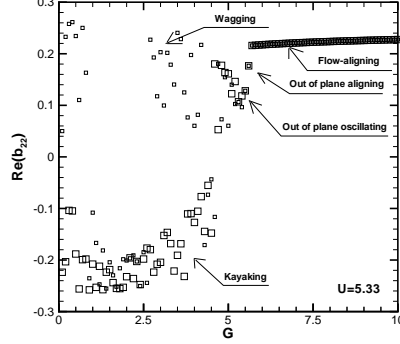


FIG. 4.4. Snapshot of $Re[b_{22}]$ at time $t = 2000$ for two different initial distribution functions for $U = 5.33$.

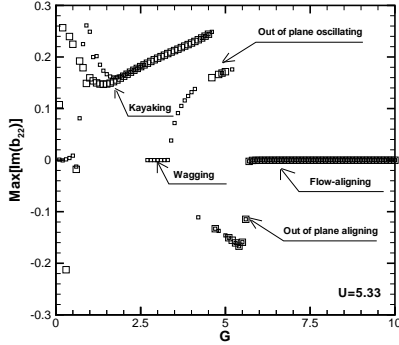


FIG. 4.5. Maximum of $Im[b_{22}]$ over the last several time periods toward $t = 2000$ for two different initial distribution functions for $U = 5.33$.

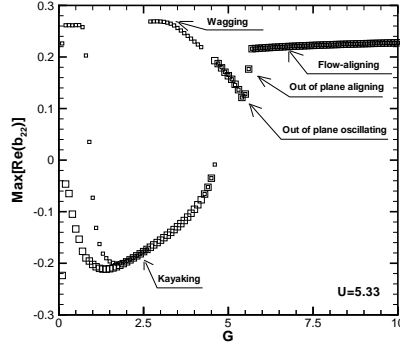


FIG. 4.6. Maximum of $Re[b_{22}]$ over the last several time periods toward $t = 2000$ for two different initial distribution functions for $U = 5.33$.

N_2 is opposite in sign to N_1 except at shear rates close to those at which N_1 changes sign. Figure 4.14 shows the dimensionless first and second normal stress difference N_1, N_2 as functions of shear rate G for $U = 6$.

The polymeric solutions display shear thinning: as the fluid is subjected to increasing shear rates, the viscosity τ_{13}/G decreases colortonically. This phenomenon of shear thinning is a benefit for polymer processing, as it relieves the stresses in these highly viscous fluids in high shear regions within process flow equipment. Figure 4.15 shows the viscosity versus the shear rate for $U = 6$. Finite jumps are observed near $G = 1.7$ and $G = 5.4$ in the figure 4.15, it is apparent that the flow induces a phase

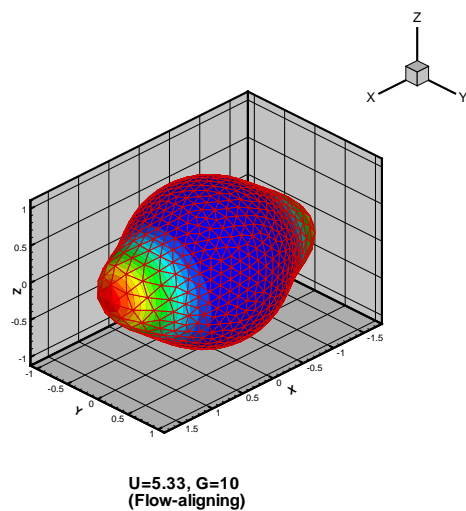


FIG. 4.7. The distribution function for $U = 5.33$ and $G = 10$. It can be seen that the director is along the x axis (the flow velocity direction). This is why this solution is called “flow-aligning”

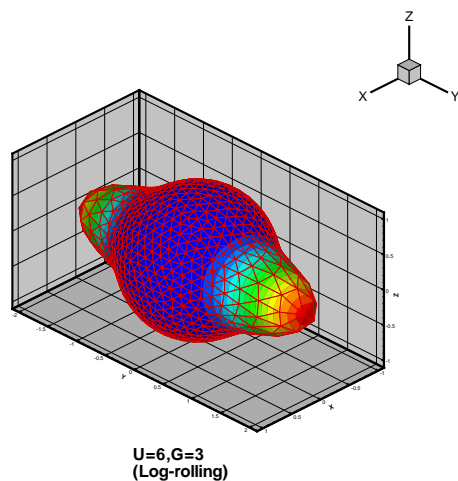


FIG. 4.8. The distribution function for $U = 6$ and $G = 3$. It can be seen that the director is along the y axis (the vorticity direction). This solution is called “log-rolling”.

transition. An infinitesimal increase of the shear rate induces a finite jump to any quantity depending on the distribution function. Figure 4.16 to 4.19 show the real and imaginary part of b_{22} for $U = 6$. The jumps appear at the transition points from tumbling to log-rolling and from log-rolling to wagging.

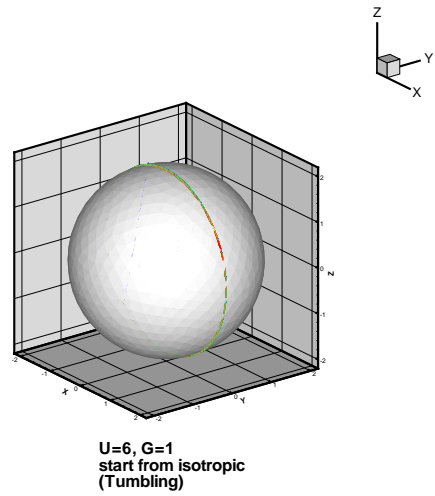


FIG. 4.9. The evolution of directors for $U = 6$ and $G = 1$. The initial distribution function is isotropic. It can be seen that from some moment on, the director begins to tumble in the shear plane (x - z plane). This solution is called “tumbling”.

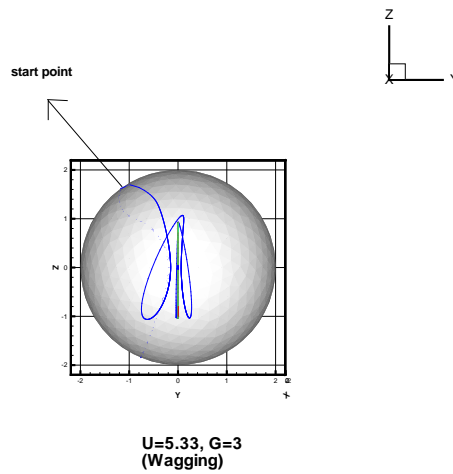


FIG. 4.10. The evolution of directors for $U = 5.33$ and $G = 3$. It can be seen that from some moment on, the director begins to oscillate near the flow direction (x axis) in the shear plane (x - z plane). This solution is called “wagging”.

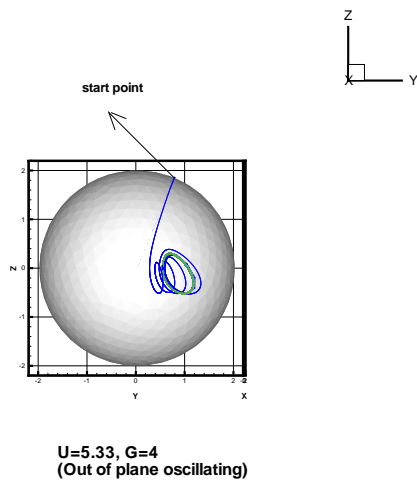


FIG. 4.11. The evolution of directors for $U = 5.33$ and $G = 4$. It can be seen that from some moment on, the director begins to rotate around an axis not in the shear plane (x - z plane). Thus this solution is called “Out of plane oscillating”.

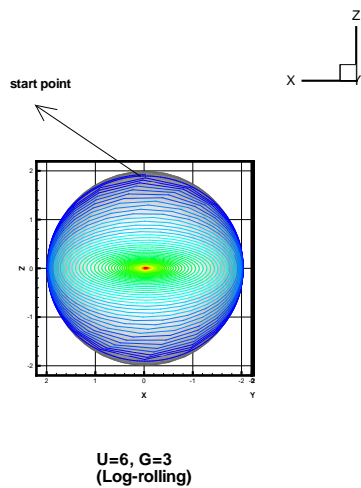


FIG. 4.12. The evolution of directors for $U = 6$ and $G = 3$. It can be seen that the director eventually converges to the y axis. This solution is called “log-rolling”.

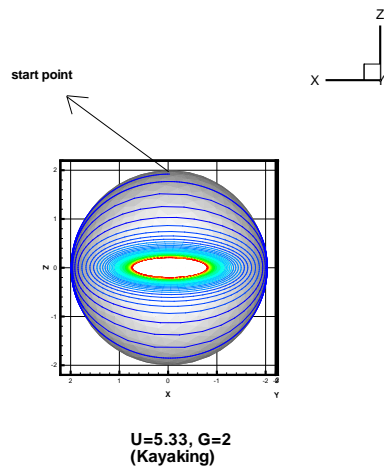


FIG. 4.13. The evolution of directors for $U = 5.33$ and $G = 2$. It can be seen that from some moment on, the director begin to rotate around the y axis. This solution is called “Kayaking”.

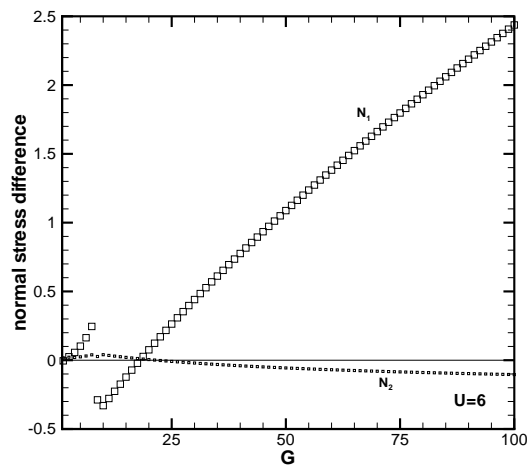


FIG. 4.14. First and second normal stress vs shear rate G for $U = 6$.

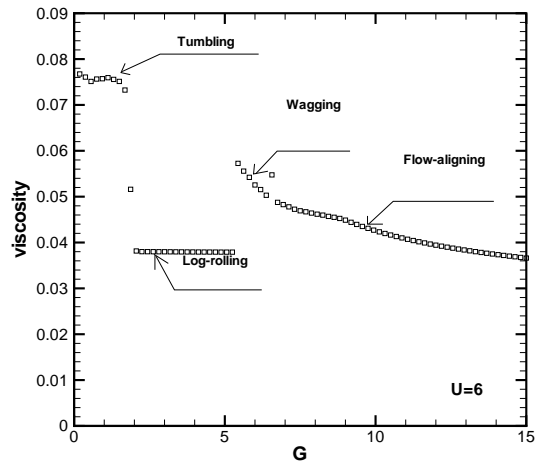


FIG. 4.15. Viscosity vs shear rate G for isotropic initial distribution function for $U = 6$.

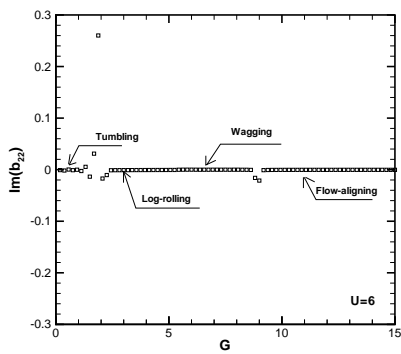


FIG. 4.16. Snapshot of $\text{Im}[b_{22}]$ at time $t = 2000$ for isotropic initial distribution function for $U = 6$.

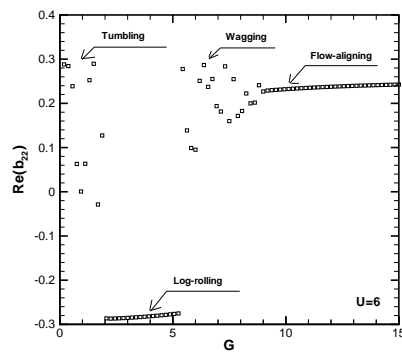


FIG. 4.17. Snapshot of $\text{Re}[b_{22}]$ at time $t = 2000$ for isotropic initial distribution function for $U = 6$.

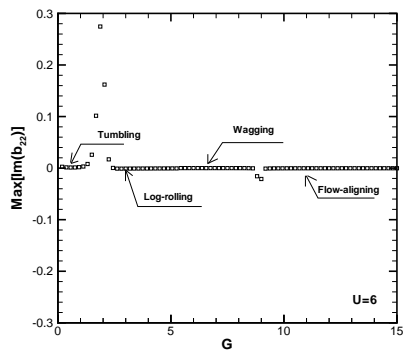


FIG. 4.18. Maximum of $\text{Im}[b_{22}]$ over the last several time periods toward $t = 2000$ for isotropic initial distribution function for $U = 6$.

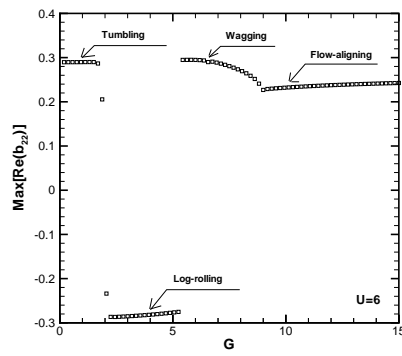


FIG. 4.19. Maximum of $\text{Re}[b_{22}]$ over the last several time periods toward $t = 2000$ for isotropic initial distribution function for $U = 6$.

5. Conclusion . In this work the Doi model for rodlike polymers under shear flows has been studied. The finite element method on sphere is developed. A rather complete characterization of the model predictions is presented, which is consistent with previous work. One interesting result, which may induce the numerical difficulty and stimulate experimental efforts, is the jump of viscosity coming from the flow induced phase transition.

Acknowledgments. We are grateful to Weinan E for helpful discussions. P. Zhang is partially supported by the special funds for Major State Research Projects G1999032804 and National Science Foundation of China for Distinguished Young Scholars 10225103.

REFERENCES

- [1] R. B. BIRD, O. HASSAGER, R. C. ARMSTRONG AND C. F. CURTISS, DYNAMICS OF POLYMERIC LIQUIDS; VOL. 2: KINETIC THEORY (2ND ED.), WILEY-INTERSCIENCE, 1987.
- [2] M. DOI, S. F. EDWARDS, THE THEORY OF POLYMER DYNAMICS, OXFORD UNIVERSITY PRESS, (1986).
- [3] Q. DU, M. GUNZBURGER, *Grid generation and optimization based on centroidal Voronoi tessellations*, APPLIED MATHEMATICS AND COMPUTATION **113** (2002) 591-607.
- [4] W. E, H. ZHANG AND P. ZHANG, *Study of rigid rodlike models for polymers*, PREPRINT, (2003).
- [5] J. ERICKSEN, *Liquid crystals with variable degree of orientation*, ARCH. RAT. MECH. ANAL., **113** (1991) 97-120.
- [6] V. FARAONI, M. GROSSO, S. CRESCITELLI AND P.L. MAFFETTONE, *The rigid-rod model for nematic polymers: an analysis of the shear flow problem*, J. RHEOL., **43** (1999) 829-843.
- [7] P. G. DE GENNES AND J. PROST, THE PHYSICS OF LIQUID CRYSTALS, SECOND EDITION, OXFORD SCIENCE PUBLICATIONS, 1993.
- [8] G. MARRUCCI AND P. L. MAFFETTONE, *Description of the liquid crystalline phase of rodlike polymers at high shear rates*, MARCOMOLECULES, **22** (1989) 4076-4082.
- [9] R. G. LARSON, *Arrested tumbling in shearing flows of liquid crystalline polymers*, MARCOMOLECULES, **23** (1990) 3983-3992.
- [10] R. G. LARSON AND D. W. MEAD, *The Ericksen number and Deborah number cascades in sheared polymeric nematics*, LIQ. CRYST., **15** (1993) 151-169.
- [11] R. G. LARSON AND D. W. MEAD, *Development of orientation and texture during shearing of liquid-crystalline polymers*, LIQ. CRYST., **12** (1992) 75-768.
- [12] R. G. LARSON AND H. C. ÖTTINGER, *The effect of molecular elasticity on out-of-plane orientations in shearing flows of the liquid crystalline polymers*, MARCOMOLECULES, **24** (1991) 6270-6282.
- [13] M. LASO AND H. C. ÖTTINGER, *Calculation of viscoelastic flow using molecular models: the CONNFFESSIT approach*, J. NON-NEWTONIAN FLUID MECH. **47** (1993), 1-20.
- [14] R. NAYAK, *Molecular simulation of liquid crystal polymer flow: a wavelet-finite element analysis*, PHD THESIS, MIT, 1998.
- [15] A. D. REY AND T. TSUJI, *Orientation mode selection mechanisms for sheared nematic liquid crystalline materials*, PHYSICAL REVIEW E, **57(5)** (1998) 5610-5625.
- [16] A. D. REY AND T. TSUJI, *Recent advances in theoretical liquid crystal rheology*, MACROMOL. THEORY SIMUL., **7** (1998) 623-639.
- [17] R. SADOURNY, A. ARAKAWA AND Y. MINTZ, *Integration of the nondivergent barotropic vorticity equation with an icosahedralhexagonal grid for the sphere*, MON. WEA. REV., **96** (1968) 351-356.
- [18] J. K. C. SUEN, Y. L. JOO AND R. C. ARMSTRONG, *Molecular orientation effects in viscoelasticity*, ANNU. REV. FLUID MECH. **34** (2002), 417-444.
- [19] D. L. WILLIAMSON, *Integration of the barotropic vorticity equation on a spherical geodesic grid*, TELLUS, **20** (1968), 642-653.
- [20] P. ZHANG, F. OTTO AND W. E, *Multi-Scale Modeling of the Dynamics of Disclinations and Microstructures in Liquid Crystal Polymer Flow*, PREPRINT, (2003).